Signatures of optical conductivity in double-layer graphene excitonic condensate

Van-Nham Phan[1,2,*] and Quoc-Huy Ninh[3]

[1]*Institute of Research and Development, Duy Tan University, 3 Quang Trung, 550000 Danang, Vietnam*
[2]*Faculty of Natural Sciences, Duy Tan University, Da Nang 550000, Vietnam*
[3]*Natural faculty of science, Langson college of education, Chi Lang, 240000 Langson, Vietnam*

(Received 26 August 2020; revised 10 March 2021; accepted 16 March 2021; published 29 March 2021)

Signatures of the excitonic condensation state and its optical properties in biased double-layer graphene (DLG) are discussed. In the framework of the generic bilayer graphene model involving a Coulomb interaction between electrons in one layer and holes in the opposite layer, we have derived a set of self-consistent equations determining the excitonic condensate order parameter by use of the projector-based renormalization method. Based on the Kubo theory of the linear optical response, a formula of the optical conductivity is also obtained with full contributions of the quantum fluctuations. Our results elucidate a possibility of the excitonic condensation formation in the biased system once the dielectric thickness is sufficiently small. As a function of the external electric field, the excitonic condensation dome suppresses rapidly as enlarging the dielectric thickness. The impression of the dielectric thickness and external electric field affecting the excitonic condensate is also addressed in the signature of the optical conductivity. Our findings are worthwhile to understand the formation and stability of the excitonic condensation states not only in DLG but also in other double-layer systems or in semimetal-semiconductor transition materials.

DOI: 10.1103/PhysRevB.103.125156

I. INTRODUCTION

The coherent state of a homogeneously bosonic quasiparticle system driven by electronic correlations is one of the most fundamental phenomena in condensed matter physics. At a sufficiently small temperature, the amount of the quasiparticles might stabilize in a macroscopic coherent state following the Bose-Einstein condensation (BEC) theory [1,2]. One of the most perspective candidates for observing the BEC at a large temperature is the exciton—an extremely small effective mass bosonic quasiparticle formed by a composition of electrons and holes driven by the Coulomb interaction. The excitons have been predicted to be able to condense in a macroscopic phase-coherent so-called excitonic condensation state since the '60s of the last century [3,4], however, experimental attestations of the coherent state are still modest. So far, the excitonic condensation state has been observed experimentally in some transition-metal dichalcogenides (TMDs) [5,6] and in some double-layer systems such as semiconductor double quantum wells [7,8], double-bilayer graphene [9,10], and double-layer graphene (DLG) [11].

Graphene and its based structures are most likely the building blocks of future nanoelectronic devices [12–14]. Single-layer graphene (SLG) is an exact two-dimensional system [15,16] that is similar to unbiased bilayer graphene (BLG), consisting of two AB-stacked, chemically bound graphene monolayers [17,18]. More interestingly, one finds another graphene-based structure like BLG but two graphene sheets are separated by a dielectric so the tunneling between the layers can be ignored [19–22]. That structure, so-called DLG, has attracted much interest because the charge carrier concentration of an individual layer in the system can be controlled simply by the application of a gate voltage [18,23]. This electric-field effect is fundamental for potential technological applications. Once a gate bias is applied across the two sheets, an attractive Coulomb interaction between the excess electrons on one layer and holes on the opposite layers raises the possibility of the formation of electron-hole bound states [19,20,24–28]. In a double-layer system, electrons and holes are separated by a thickness dielectric layer, they thus have less probability to recombine or an exciton can live longer than that formed in the normal TMD [7,8]. Experimental observation of excitonic condensation in a DLG is thus more accessible. The excitonic condensation state in DLG has been triggered like a superfluid state of Cooper pairs in the microscopic Bardeen-Cooper-Schrieffer (BCS) theory [25,26,29] that has been experimentally typified recently in Ref. [11].

To examine in more detail the excitonic condensate in DLG, especially its optical response signatures, in the present paper, we use the projector-based renormalization method (PRM) adapting to a generic graphene bilayer model, taking into account the Coulomb interaction between an electron in one layer and a hole in the opposite layer. The PRM starts from a many-particle Hamiltonian. By using a sequence of the unitary transformations, a nondiagonal part of the Hamiltonian is integrated out and one obtains a completely renormalized Hamiltonian in a diagonal form. The physical relevant quantities, therefore, would be more simply calculated in the form of the renormalized Hamiltonian. Note here that the Hilbert space is not reduced by the sequence of the unitary transformations; the eigenspectrum of the original Hamiltonian thus remains after the renormalization process [30]. At first glance, the PRM is similar to Wilson's

*Corresponding author: phanvannham@duytan.edu.vn

renormalization group approach [31–33]. However, there are some big differences between them. If the aim of Wilson's approach is to reduce the size of the Hamiltonian matrix by keeping its smallest eigenvalues, the PRM remains the Hamiltonian size but eliminates the off-diagonal terms. With the reduced size, the Hamiltonian matrix in Wilson's approach might be solved numerically. The energy cutoff in Wilson's approach indicating the renormalized Hamiltonian matrix size, therefore, is finite. Meanwhile, by eliminating the off-diagonal parts, the renormalized Hamiltonian in the PRM might be diagonal, thus relevant physical quantities are easily evaluated. In PRM, the energy cutoff indicates the energy transitions induced by the off-diagonal parts and it might be zero and the renormalized Hamiltonian is diagonal. In both of the methods, the renormalization is taken by using the unitary transformation to derive the finally renormalized Hamiltonian and the unsolvable parts are eliminated by using the projector operators. Note that our PRM used here has some connections to Wegner's continuous flow equation method [34] if a special case of the unitary transformation generator is chosen [30]. The latter approach is similar to the similarity transformation introduced by Glazek and Wilson but applied for many-particle physics (Glazek and Wilson originally introduced the approximation for the field of high-energy physics) [35,36]. Our approach, therefore, is much connected with the similarity transformation introduced by Glazek and Wilson and the continuous flow equation method of Wegner (see recent review in Ref. [30]), rather than Wilson's renormalization group approach.

The PRM has been shown to be applicable to address complex superfluid phase structures in various many-particle quantum systems such as excitonic condensate in TMDs [37,38], excitonic-polaritonic condensation in microcavities [39,40], or unconventional superconducting states in high-T_c cuprates or in heavy-fermion systems [41,42]. In our calculations, we have supposed that electron-hole pair formation and condensation might appear in the DLG system at least at zero temperature if a gate bias is applied. In doing so, we expect to derive a set of self-consistent equations in the framework of the PRM permitting us to solve numerically the excitonic condensate order parameters once the quantum fluctuations are taken into account.

To inspect in more detail the nature of the excitonic condensation state in the DLG, in this paper, we also examine the optical response of the system in the condensation state. The optical response has become one of the most effective tools, providing important insight into the excitonic condensation state in a system. Indeed, by using the density functional theory and density-matrix renormalization group method, experimental optical conductivity spectra have been analyzed and reveal that the preformed exciton might occur in the semimetal Ta_2NiSe_5 at a temperature larger than excitonic condensate critical value [43]. That is in contrast with the conventional picture that the preformed excitons are found only in semiconductor materials [38,44]. Recently, the collective modes of the excitonic condensation state in Ta_2NiSe_5 were also discussed in a signature of the optical conductivity [45,46]. The optical response has been used to address the excitonic condensation state in doped SLG [47] and BLG [48] but not in DLG, in our knowledge so far. However, in a signature of the frequency dependence of transmission, reflection, and absorption coefficients, some dynamical properties of the electron-hole pairs have been discussed [49–51]. The stability of the excitonic condensation state in DLG in a signature of the optical response thus remains an open issue.

Our main interests here are the effects of the dielectric thickness and the external electric field regarding the optical properties in the excitonic condensate DLG. In the feature of the PRM, we derive an analytical formula for the real part of the optical conductivity based on the linear optical response theory [52]. The signature of the optical properties of the system in the condensation state then is addressed. Analyzing the optical conductivity spectrum might allow us to examine the bound electron-hole pair state preceding the stability of the condensation state. Indeed, the real part of the optical conductivity rises—a sharp peak at a frequency equal to the band gap or twice the excitonic order parameter at the Fermi level. Our findings are worthwhile to understand the formation and stability of the excitonic condensation states not only in DLG but also in the other double-layer systems or in emimetal-semiconductor transition materials.

The present paper is organized as follows. In Sec. II, we introduce the generic BLG model applied for the DLG in which the Coulomb interaction between electrons on one layer with holes in the opposite layer is involved. Next, in Sec. III, the PRM is proposed to solve the model described in the previous section. Here, explicit renormalized equations and a set of self-consistent equations determining the excitonic condensate order parameter are given. In this section, we also present the analytical result for the real part of the optical conductivity in the framework of the PRM. Section IV shows the numerical results and their discussions. Finally, the conclusions can be found in Sec. V.

II. MODEL

To model the electron-hole system in a DLG, first we assume that the two graphene sheets are stacked in hexagonal and separated by a dielectric thickness of d. A gate-induced potential difference between the two layers V_g is applied, then an electric field $E_{ext} = V_g/(ed)$ is formed inside the structure. The gate-induced potential difference or the electric field can be used to tune the chemical potential $\mu = V_g/2$ [25]. The finite potential difference releases an opposite charge density in the two layers, so-called upper (n-type) and lower (p-type) layers. Assuming the DLG system is neutral, then the Fermi level lies symmetrically in the conduction band of the upper layer and in the valence band of the lower layer. In analogy to the situation in the electron-hole system in a semimetal-semiconductor transition [3,4], in the present paper, we use the electron instead of the hole representation for the valance band. The hole representation might be delivered simply by the electron-hole transformation. In the low-energy approximation, the filled valence and empty conduction bands can be omitted and the conducting electron system of the valance and hole bands in DLG can be described by the following

Hamiltonian:

$$\mathcal{H} = g_s \sum_{\mathbf{k}} \varepsilon^{+}_{\mathbf{k}} a^{\dagger}_{\mathbf{k}} a_{\mathbf{k}} + g_s \sum_{\mathbf{k}} \varepsilon^{-}_{\mathbf{k}} b^{\dagger}_{\mathbf{k}} b_{\mathbf{k}} + \frac{g_s}{N} \sum_{\mathbf{k}_1\mathbf{k}_2,\mathbf{q}\neq 0} U_{\mathbf{k}_1\mathbf{k}_2\mathbf{q}}\, a^{\dagger}_{\mathbf{k}_1+\mathbf{q}} a_{\mathbf{k}_1} b^{\dagger}_{\mathbf{k}_2-\mathbf{q}} b_{\mathbf{k}_2}, \quad (1)$$

where $g_s = 2$ allows for the spin degeneracy. The first two terms in Eq. (1) indicate the noninteracting electron system in momentum space with $a^{\dagger}_{\mathbf{k}}$ ($a_{\mathbf{k}}$) and $b^{\dagger}_{\mathbf{k}}$ ($b_{\mathbf{k}}$) being the creation (annihilation) operators of electron in the conduction and the valance bands at momentum $\mathbf{k}$, respectively. The band dispersions $\varepsilon^{\pm}_{\mathbf{k}}$ in the tight-binding approximation read

$$\varepsilon^{\pm}_{\mathbf{k}} = \pm\gamma_0 \left[1 + 4\cos^2\frac{k_y}{2} + 4\cos\frac{k_y}{2}\cos\frac{\sqrt{3}k_x}{2} \right]^{1/2} \mp \mu, \quad (2)$$

with γ_0 denoting the nearest-neighbor transfer amplitude ($\gamma_0 \simeq 2.8$ eV [12]) and μ is the chemical potential. The last term in Eq. (1) describes the long-ranged Coulomb interaction between conduction-band electrons in one layer and valence-band electrons in the opposite layer with

$$U_{\mathbf{k}_1\mathbf{k}_2\mathbf{q}} = \kappa \frac{e^{-d|\mathbf{q}|}}{|\mathbf{q}|} \cos\frac{\phi_1}{2}\cos\frac{\phi_2}{2} \quad \text{with} \quad \kappa = g_s \frac{2\pi e^2}{\epsilon}, \quad (3)$$

depending on the dielectric constant ϵ of a medium barrier between two graphene sheets and distance d between them. Here, $\phi_i = \theta_{\mathbf{k}_i} - \theta_{\mathbf{k}_i+\mathbf{q}}$, with $\theta_{\mathbf{k}} = \mathrm{atan}(k_y/k_x)$, is the scattering angle [20]. In the Hamiltonian written in Eq. (1) we have omitted the intralayer Coulomb repulsion between on-layer electrons that manifests itself simply by a screening of the interlayer Coulomb interaction.

To describe the excitonic condensation state, a spontaneously broken symmetry with respect to the stability of the coherent state of electron-hole pairs needs to appear in the original Hamiltonian. In doing so, a hybridization between conduction-band electrons and valence-band electrons must be considered. Practically, we rewrite the Hamiltonian Eq. (1) in the representation of a normal-ordered form in a way that an arbitrary operator $\mathcal{A}$ would be written by $A =: \mathcal{A} : + \langle \mathcal{A} \rangle$. The Hamiltonian in Eq. (1) then is

$$\mathcal{H} = \mathcal{H}_0 + \mathcal{H}_1, \quad (4)$$

where

$$\mathcal{H}_0 = \sum_{\mathbf{k}} [\varepsilon^{+}_{\mathbf{k}} a^{\dagger}_{\mathbf{k}} a_{\mathbf{k}} + \varepsilon^{-}_{\mathbf{k}} b^{\dagger}_{\mathbf{k}} b_{\mathbf{k}} + (\Delta_{\mathbf{k}} b^{\dagger}_{\mathbf{k}} a_{\mathbf{k}} + \mathrm{H.c.})] \quad (5)$$

and

$$\mathcal{H}_1 = \frac{1}{N} \sum_{\mathbf{k}_1\mathbf{k}_2,\mathbf{q}\neq 0} U_{\mathbf{k}_1\mathbf{k}_2\mathbf{q}} : a^{\dagger}_{\mathbf{k}_1+\mathbf{q}} a_{\mathbf{k}_1} b^{\dagger}_{\mathbf{k}_2-\mathbf{q}} b_{\mathbf{k}_2} : . \quad (6)$$

Here, we have decomposed the Hamiltonian into two parts, the noninteracting part $\mathcal{H}_0$ and the perturbation $\mathcal{H}_1$ containing the fluctuating part of the Coulomb interaction. Note here that the Hamiltonian has also been written in the unit of the spin degeneracy g_s and all constants have been eliminated. In Eq. (5), we have defined

$$\Delta_{\mathbf{k}} = -\frac{\kappa}{N} \sum_{\mathbf{q}} \frac{e^{-d|\mathbf{q}|}}{|\mathbf{q}|} \frac{(1+\cos\phi)}{2} \delta_{\mathbf{k}+\mathbf{q}} \quad (7)$$

to indicate the spontaneous symmetry breaking with $\phi = \theta_{\mathbf{k}+\mathbf{q}} - \theta_{\mathbf{k}}$ and $\delta_{\mathbf{k}+\mathbf{q}} = \langle a^{\dagger}_{\mathbf{k}+\mathbf{q}} b_{\mathbf{k}+\mathbf{q}} \rangle$. Because the Coulomb interaction is long ranged, by excluding the $\mathbf{q} = 0$ component (comprising the jellium background), no Hartree contribution to the one-particle energies is involved. That is differentfrom the case of the local situation as in the extended Falicov-Kimball model [37,38,40].

III. THEORETICAL APPROACH

A. Renormalized Hamiltonian

In the present work, the Hamiltonian written in Eq. (4) is analyzed in the framework of the PRM, a special case of the generalized diagonalization scheme recently reviewed in Ref. [30]. The renormalization scheme is started from the ansatz of a renormalized Hamiltonian at a cutoff λ,

$$\mathcal{H}_\lambda = \mathcal{H}_{0,\lambda} + \mathcal{H}_{1,\lambda}, \quad (8)$$

where

$$\mathcal{H}_{0,\lambda} = \sum_{\mathbf{k}} [\varepsilon^{+}_{\mathbf{k},\lambda} a^{\dagger}_{\mathbf{k}} a_{\mathbf{k}} + \varepsilon^{-}_{\mathbf{k},\lambda} b^{\dagger}_{\mathbf{k}} b_{\mathbf{k}} + (\Delta_{\mathbf{k},\lambda} b^{\dagger}_{\mathbf{k}} a_{\mathbf{k}} + \mathrm{H.c.})] \quad (9)$$

and

$$\mathcal{H}_{1,\lambda} = \frac{\mathbf{P}_\lambda}{N} \sum_{\mathbf{k}_1\mathbf{k}_2,\mathbf{q}\neq 0} U_{\mathbf{k}_1\mathbf{k}_2\mathbf{q}} : a^{\dagger}_{\mathbf{k}_1+\mathbf{q}} a_{\mathbf{k}_1} b^{\dagger}_{\mathbf{k}_2-\mathbf{q}} b_{\mathbf{k}_2} :, \quad (10)$$

with all the parameters of $\mathcal{H}_{0,\lambda}$ depending on the cutoff λ and the projection operator $\mathbf{P}_\lambda$ defined as $\mathbf{P}_\lambda \mathcal{H}_\lambda = \Theta(\lambda - |\omega_\lambda|)\mathcal{H}_\lambda$ projects on all low-energy transitions with respect to the unperturbed Hamiltonian $\mathcal{H}_{0,\lambda}$, ω_λ. Then a completely renormalized Hamiltonian, $\tilde{\mathcal{H}} = \mathcal{H}_{\lambda=0}$, can be found by using a general flow equation:

$$\mathcal{H}_{\lambda-\Delta\lambda} \approx \mathcal{H}_{0,\lambda} + \mathcal{H}_{1,\lambda} + [X_{\lambda,\Delta\lambda}, \mathcal{H}_{0,\lambda} + \mathcal{H}_{1,\lambda}], \quad (11)$$

where a generator operator $X_{\lambda,\Delta\lambda}$ is defined as

$$X_{\lambda,\Delta\lambda} = \frac{1}{N} \sum_{\mathbf{k}_1\mathbf{k}_2,\mathbf{q}\neq 0} \alpha_{\mathbf{k}_1\mathbf{k}_2\mathbf{q}}(\lambda,\Delta\lambda) : a^{\dagger}_{\mathbf{k}_1+\mathbf{q}} a_{\mathbf{k}_1} b^{\dagger}_{\mathbf{k}_2-\mathbf{q}} b_{\mathbf{k}_2} :, \quad (12)$$

with the prefactor given by

$$\alpha_{\mathbf{k}_1\mathbf{k}_2\mathbf{q}}(\lambda,\Delta\lambda) = \frac{\Theta_{\mathbf{k}_1\mathbf{k}_2\mathbf{q},\lambda}\left(1 - \Theta_{\mathbf{k}_1\mathbf{k}_2\mathbf{q},\lambda-\Delta\lambda}\right) U_{\mathbf{k}_1\mathbf{k}_2\mathbf{q}}}{\varepsilon^{+}_{\mathbf{k}_1+\mathbf{q},\lambda} - \varepsilon^{+}_{\mathbf{k}_1,\lambda} + \varepsilon^{-}_{\mathbf{k}_2-\mathbf{q},\lambda} - \varepsilon^{-}_{\mathbf{k}_2,\lambda}} \quad (13)$$

and

$$\Theta_{\mathbf{k}_1\mathbf{k}_2\mathbf{q},\lambda} = \Theta\left(\lambda - \left|\varepsilon^{+}_{\mathbf{k}_1+\mathbf{q},\lambda} - \varepsilon^{+}_{\mathbf{k}_1,\lambda} + \varepsilon^{-}_{\mathbf{k}_2-\mathbf{q},\lambda} - \varepsilon^{-}_{\mathbf{k}_2,\lambda}\right|\right), \quad (14)$$

which restricts transitions to excitation energies smaller than λ.

To arrive at the completely renormalized Hamiltonian, one needs a set of renormalization equations showing a λ dependence of the model parameters. The result on the right-hand side of Eq. (11) must be compared with the generic forms in Eqs. (9) and (10) of $\mathcal{H}_\lambda$ (with λ replaced by $\lambda - \Delta\lambda$) when it is written in terms of the original λ-independent variables $a^{(\dagger)}_{\mathbf{k}}$ and $b^{(\dagger)}_{\mathbf{k}}$. This leads to the following renormalization equations

for the parameters of $\mathcal{H}_{0,\lambda}$:

$$\begin{aligned}\varepsilon^{+}_{\mathbf{k},\lambda-\Delta\lambda} - \varepsilon^{+}_{\mathbf{k},\lambda} =& \frac{1}{N^2}\sum_{\mathbf{pq}}\{U_{\mathbf{k},\mathbf{p}+\mathbf{q},\mathbf{q}}\alpha_{\mathbf{k}+\mathbf{q},\mathbf{p},-\mathbf{q}}(\lambda,\Delta\lambda)\\ &\times\left[n^{b}_{\mathbf{p}+\mathbf{q}}\left(1-n^{b}_{\mathbf{p}}\right)-n^{a}_{\mathbf{k}+\mathbf{q}}\left(n^{b}_{\mathbf{p}}-n^{b}_{\mathbf{p}+\mathbf{q}}\right)\right]\\ &-U_{\mathbf{k}-\mathbf{q},\mathbf{p}+\mathbf{q},\mathbf{q}}\alpha_{\mathbf{k},\mathbf{p},-\mathbf{q}}(\lambda,\Delta\lambda)\\ &\times\left[n^{b}_{\mathbf{p}+\mathbf{q}}\left(1-n^{b}_{\mathbf{p}}\right)+\left(1-n^{a}_{\mathbf{k}-\mathbf{q}}\right)\left(n^{b}_{\mathbf{p}}-n^{b}_{\mathbf{p}+\mathbf{q}}\right)\right]\},\end{aligned} \tag{15}$$

$$\begin{aligned}\varepsilon^{-}_{\mathbf{k},\lambda-\Delta\lambda} - \varepsilon^{-}_{\mathbf{k},\lambda} =& \frac{1}{N^2}\sum_{\mathbf{pq}}\{U_{\mathbf{p},\mathbf{k},\mathbf{q}}\alpha_{\mathbf{p}+\mathbf{q},\mathbf{k}-\mathbf{q},-\mathbf{q}}(\lambda,\Delta\lambda)\\ &\times\left[n^{a}_{\mathbf{p}+\mathbf{q}}\left(1-n^{a}_{\mathbf{p}}\right)+\left(n^{a}_{\mathbf{p}}-n^{a}_{\mathbf{p}-\mathbf{q}}\right)\left(1-n^{b}_{\mathbf{k}+\mathbf{q}}\right)\right.\\ &-U_{\mathbf{p},\mathbf{k}+\mathbf{q},\mathbf{q}}\alpha_{\mathbf{p}+\mathbf{q},\mathbf{k},-\mathbf{q}}(\lambda,\Delta\lambda)\\ &\times\left[n^{a}_{\mathbf{p}+\mathbf{q}}\left(1-n^{a}_{\mathbf{p}}\right)-\left(n^{a}_{\mathbf{p}}-n^{a}_{\mathbf{p}+\mathbf{q}}\right)n^{b}_{\mathbf{p}+\mathbf{q}}\right]\},\end{aligned} \tag{16}$$

$$\begin{aligned}\Delta_{\mathbf{k},\lambda-\Delta\lambda} - \Delta_{\mathbf{k},\lambda} =& -\frac{1}{N}\sum_{\mathbf{p}}\Delta_{\mathbf{k},\lambda}\alpha_{\mathbf{k},\mathbf{k}+\mathbf{p},\mathbf{p}}(\lambda,\Delta\lambda)\left(n^{a}_{\mathbf{k}+\mathbf{p}}-n^{b}_{\mathbf{k}+\mathbf{p}}\right)\\ &-\frac{1}{N^2}\sum_{\mathbf{pq}}\delta_{\mathbf{p}+\mathbf{q}}\left[U_{\mathbf{k},\mathbf{p}+\mathbf{q},\mathbf{q}}\alpha_{\mathbf{k}+\mathbf{q},\mathbf{p},\mathbf{p}-\mathbf{k}}(\lambda,\Delta\lambda)\right.\\ &\times\left(1-n^{b}_{\mathbf{p}}+n^{b}_{\mathbf{k}+\mathbf{q}}\right)\\ &-U_{\mathbf{p},\mathbf{k}+\mathbf{q},\mathbf{q}}\alpha_{\mathbf{k},\mathbf{p}+\mathbf{q},\mathbf{p}-\mathbf{k}}(\lambda,\Delta\lambda)\left(1-n^{a}_{\mathbf{p}}+n^{a}_{\mathbf{k}+\mathbf{q}}\right)\Big].\end{aligned} \tag{17}$$

The quantities $n^{a}_{\mathbf{k}}$, $n^{b}_{\mathbf{k}}$ are occupation numbers for electrons in the conduction and valance bands,

$$n^{a}_{\mathbf{k}} = \langle a^{\dagger}_{\mathbf{k}}a_{\mathbf{k}}\rangle\,, \quad n^{b}_{\mathbf{k}} = \langle b^{\dagger}_{\mathbf{k}}b_{\mathbf{k}}\rangle, \tag{18}$$

and have to be evaluated separately. To solve numerically the above difference equations, one needs the initial values of the renormalization parameters at $\lambda = \Lambda$, they are those with regarding to the original Hamiltonian $\mathcal{H}$, i.e.,

$$\varepsilon^{\pm}_{\mathbf{k},\Lambda} = \varepsilon^{\pm}_{\mathbf{k}}\,, \quad \Delta_{\mathbf{k},\mathbf{\Lambda}} = \Delta_{\mathbf{k}}. \tag{19}$$

Supposing the expectation values $n^{a}_{\mathbf{k}}$, $n^{b}_{\mathbf{k}}$, and $\delta_{\mathbf{k}}$ in Eqs. (15)–(17) are already known, the renormalization equations can be integrated between $\lambda = \Lambda$ and $\lambda = 0$. In this way, we arrive at all the renormalization parameters at $\lambda = 0$ or the fully renormalized Hamiltonian $\tilde{\mathcal{H}} := \mathcal{H}_{\lambda=0} = \mathcal{H}_{0,\lambda=0}$ is obtained:

$$\tilde{\mathcal{H}} = \sum_{\mathbf{k}}\tilde{\varepsilon}^{+}_{\mathbf{k}}a^{\dagger}_{\mathbf{k}}a_{\mathbf{k}} + \sum_{\mathbf{k}}\tilde{\varepsilon}^{-}_{\mathbf{k}}b^{\dagger}_{\mathbf{k}}b_{\mathbf{k}} + \sum_{\mathbf{k}}\tilde{\Delta}_{\mathbf{k}}(a^{\dagger}_{\mathbf{k}}b_{\mathbf{k}} + \text{H.c.}). \tag{20}$$

The tilde symbols denote the fully renormalized quantities at $\lambda = 0$. All excitations from $\mathcal{H}_{1,\lambda}$ with nonzero energies have been eliminated. They give rise to the renormalization of $\mathcal{H}_{0,\lambda}$. The completely renormalized Hamiltonian in Eq. (20) can be diagonalized by a Bogoliubov transformation, which gives

$$\tilde{\mathcal{H}}_{\text{dia}} = \sum_{\alpha=\pm}E^{\alpha}_{\mathbf{k}}\hat{c}^{\dagger}_{\mathbf{k}\alpha}\hat{c}_{\mathbf{k}\alpha}, \tag{21}$$

where the electronic quasiparticle energies and quasiparticles operators, respectively, read

$$E^{\pm}_{\mathbf{k}} = \frac{\tilde{\varepsilon}^{+}_{\mathbf{k}}+\tilde{\varepsilon}^{-}_{\mathbf{k}}}{2} \mp \frac{\text{sgn}(\tilde{\varepsilon}^{-}_{\mathbf{k}}-\tilde{\varepsilon}^{+}_{\mathbf{k}})}{2}W_{\mathbf{k}}\,, \tag{22}$$

with

$$W_{\mathbf{k}} = \sqrt{(\tilde{\varepsilon}^{+}_{\mathbf{k}}-\tilde{\varepsilon}^{-}_{\mathbf{k}})^2 + 4|\tilde{\Delta}_{\mathbf{k}}|^2} \tag{23}$$

and

$$\hat{c}^{\dagger}_{\mathbf{k}\alpha} = \sum_{\beta=\pm}u^{\alpha\beta}_{\mathbf{k}}c^{\dagger}_{\mathbf{k}\beta}. \tag{24}$$

Here, we have denoted $c^{\dagger}_{\mathbf{k}+} = a^{\dagger}_{\mathbf{k}}$ and $c^{\dagger}_{\mathbf{k}-} = b^{\dagger}_{\mathbf{k}}$. The prefactors $u^{\alpha\beta}_{\mathbf{k}}$ are given by

$$\begin{aligned}u^{++}_{\mathbf{k}} = -u^{--}_{\mathbf{k}} &= \frac{1}{2}\left[1+\text{sgn}(\tilde{\varepsilon}^{-}_{\mathbf{k}}-\tilde{\varepsilon}^{+}_{\mathbf{k}})\frac{\tilde{\varepsilon}^{-}_{\mathbf{k}}-\tilde{\varepsilon}^{+}_{\mathbf{k}}}{W_{\mathbf{k}}}\right]^{1/2},\\ u^{+-}_{\mathbf{k}} = u^{-+}_{\mathbf{k}} &= \frac{1}{2}\left[1-\text{sgn}(\tilde{\varepsilon}^{-}_{\mathbf{k}}-\tilde{\varepsilon}^{+}_{\mathbf{k}})\frac{\tilde{\varepsilon}^{-}_{\mathbf{k}}-\tilde{\varepsilon}^{+}_{\mathbf{k}}}{W_{\mathbf{k}}}\right]^{1/2}.\end{aligned} \tag{25}$$

The Hamiltonian written in Eq. (21) has a quadratic form that allows us to simply compute all expectation values formed with the renormalized Hamiltonian $\tilde{\mathcal{H}}$.

B. Expectation values

To solve the renormalization equations in Eqs. (15)–(17), all expectation values $n^{a}_{\mathbf{k}}$, $n^{b}_{\mathbf{k}}$, and $\delta_{\mathbf{k}}$ formed with the full Hamiltonian $\mathcal{H}$ must be evaluated. In the framework of the PRM, an expectation value formed with $\mathcal{H}$, $\langle\mathcal{A}\rangle_{\mathcal{H}}$, of an operator A can be determined by using the following identity [53]:

$$\langle\mathcal{A}\rangle_{\mathcal{H}} = \langle\mathcal{A}(\lambda-\Delta\lambda)\rangle_{\mathcal{H}_{\lambda-\Delta\lambda}} = \langle\tilde{\mathcal{A}}\rangle_{\tilde{\mathcal{H}}}. \tag{26}$$

Here, $\mathcal{A}(\lambda-\Delta\lambda) = e^{X_{\lambda,\Delta\lambda}}\mathcal{A}_{\lambda}e^{-X_{\lambda,\Delta\lambda}}$ with $X_{\lambda,\Delta\lambda}$ being the generator for the unitary transformation and $\tilde{\mathcal{A}} = \mathcal{A}(\lambda=0)$ is a completely renormalized operator. To find the expectation values in Eqs. (7) and (18), one best starts from an *ansatz* for the single fermion operators $a^{\dagger}_{\mathbf{k}}(\lambda)$ and $b^{\dagger}_{\mathbf{k}}(\lambda)$ or $c^{\dagger}_{\mathbf{k}\alpha}(\lambda)$ depending on the cutoff λ. In the second order of the fluctuation operators in Eq. (10), one might choose

$$c^{\dagger}_{\mathbf{k}\alpha}(\lambda) = x^{\alpha}_{\mathbf{k},\lambda}c^{\dagger}_{\mathbf{k}\alpha} + \frac{1}{N}\sum_{\mathbf{pq}}y^{\alpha}_{\mathbf{kpq},\lambda}c^{\dagger}_{\mathbf{k}+\mathbf{q},\alpha} : c^{\dagger}_{\mathbf{p}-\mathbf{q},-\alpha}c_{\mathbf{p},-\alpha} :, \tag{27}$$

where $x^{\alpha}_{\mathbf{k},\lambda}$ and $y^{\alpha}_{\mathbf{kpq},\lambda}$ are prefactors satisfying a condition

$$\begin{aligned}\left|x^{\alpha}_{\mathbf{k},\lambda}\right|^2 = 1 - 1/N^2\sum_{\mathbf{pq}}\left|y^{\alpha}_{\mathbf{kpq},\lambda}\right|^2\left[n^{\alpha}_{\mathbf{k}+\mathbf{q}}\left(n^{-\alpha}_{\mathbf{p}-\mathbf{q}}-n^{-\alpha}_{\mathbf{p}}\right)\right.\\ \left.+\,n^{-\alpha}_{\mathbf{p}}\left(1-n^{-\alpha}_{\mathbf{p}-\mathbf{q}}\right)\right]\end{aligned} \tag{28}$$

that is derived from the anticommutation relations for the fermion operator $[c^{\dagger}_{\mathbf{k}\alpha}(\lambda), c_{\mathbf{k}\alpha}(\lambda)]_{+} = 1$, valid for any λ. In analogy to deliver the renormalization equations for the parameters of $\mathcal{H}_{\lambda}$, one can derive renormalization equations for the prefactors that read

$$y^{\alpha}_{\mathbf{kpq},\lambda-\Delta\lambda} = y^{\alpha}_{\mathbf{kpq},\lambda} + x^{\alpha}_{\mathbf{k},\lambda}\alpha_{\mathbf{kpq}}(\lambda,\Delta\lambda). \tag{29}$$

By combination with the difference equations before in Eqs. (15)–(17), the full set of Eqs. (28) and (29) can be integrated. With the initial values

$$x^{\alpha}_{\mathbf{k}\Lambda} = 1, \quad y^{\alpha}_{\mathbf{kpq},\Lambda} = 0, \tag{30}$$

the prefactors at cutoff $\lambda = 0$ can be evaluated and one might be led to the fully renormalized one-particle operators:

$$\tilde{c}^{\dagger}_{\mathbf{k}\alpha} = \tilde{x}^{\alpha}_{\mathbf{k}} c^{\dagger}_{\mathbf{k}\alpha} + \frac{1}{N}\sum_{\mathbf{pq}} \tilde{y}^{\alpha}_{\mathbf{kpq}} c^{\dagger}_{\mathbf{k}+\mathbf{q},\alpha} : c^{\dagger}_{\mathbf{p}-\mathbf{q},-\alpha} c_{\mathbf{p},-\alpha} : . \tag{31}$$

As before, the tilde symbols denote fully renormalized quantities. With Eq. (31), the expectation values in Eqs. (18) and $\delta_{\mathbf{k}}$ can be calculated:

$$n^{\alpha}_{\mathbf{k}} = |\tilde{x}^{\alpha}_{\mathbf{k}}|^2 \tilde{n}^{\alpha}_{\mathbf{k}} + \frac{1}{N^2}\sum_{\mathbf{pq}} |\tilde{y}^{\alpha}_{\mathbf{kpq}}|^2 (1 - \tilde{n}^{-\alpha}_{\mathbf{p}}) \tilde{n}^{\alpha}_{\mathbf{k}+\mathbf{q}} \tilde{n}^{-\alpha}_{\mathbf{p}-\mathbf{q}},$$

$$\delta_{\mathbf{k}} = \tilde{x}^{\alpha}_{\mathbf{k}} \tilde{x}^{-\alpha}_{\mathbf{k}} \tilde{\delta}_{\mathbf{k}} + \frac{1}{N^2}\sum_{\mathbf{pq}} \tilde{y}^{\alpha}_{\mathbf{kpq}} \tilde{y}^{-\alpha}_{\mathbf{kp},\mathbf{k}+\mathbf{q}-\mathbf{p}} \tilde{n}^{\alpha}_{\mathbf{k}+\mathbf{q}} \tilde{n}^{-\alpha}_{\mathbf{p}-\mathbf{q}} \tilde{\delta}_{\mathbf{p}}, \tag{32}$$

where $\tilde{\delta}_{\mathbf{k}} = \langle a^{\dagger}_{\mathbf{k}} b_{\mathbf{k}} \rangle_{\tilde{\mathcal{H}}}$ and $\tilde{n}^{\alpha}_{\mathbf{k}} = \langle c^{\dagger}_{\mathbf{k}\alpha} c_{\mathbf{k}\alpha} \rangle_{\tilde{\mathcal{H}}}$ are the expectation values formed with $\tilde{\mathcal{H}}$. Because the Hamiltonian $\tilde{\mathcal{H}}$ is diagonal [see Eq. (21)], the expectation values can easily be evaluated, they read

$$\tilde{n}^{\alpha}_{\mathbf{k}} = \sum_{\alpha\beta} u^{\alpha\beta}_{\mathbf{k}} f^{F}(\tilde{E}^{\beta}_{\mathbf{k}}), \tag{33}$$

$$\tilde{\delta}_{\mathbf{k}} = -[f^{F}(\tilde{E}^{+}_{\mathbf{k}}) - f^{F}(\tilde{E}^{-}_{\mathbf{k}})]\mathrm{sgn}(\tilde{\varepsilon}^{-}_{\mathbf{k}} - \tilde{\varepsilon}^{+}_{\mathbf{k}}) \frac{\tilde{\Delta}_{\mathbf{k}}}{W_{\mathbf{k}}}. \tag{34}$$

Here, the prefactors $u^{\alpha\beta}_{\mathbf{k}}$ are defined in Eqs. (25) and $f(\tilde{E}^{\alpha}_{\mathbf{k}}) = 1/(1 + e^{\tilde{E}^{\alpha}_{\mathbf{k}}/T})$ is the Fermi function and T is the temperature. Equations (7) and (32) in combination with the renormalization Eqs. (15)–(17), (28), and (29) thus form a set of self-consistent equations that might be solved straightforwardly by a numerical method to determine the excitonic condensate order parameters in the approach of PRM.

C. Optical conductivity

To examine the optical absorption properties in the condensation state, we start from the Kubo formula of the linear response theory [52]. The real part of the optical conductivity as a function of frequency ω is thus given by

$$\sigma(\omega) = \mathrm{Re}\frac{1}{\omega}\int_0^{\infty} dt e^{i\omega t} \langle [j(t), j(0)] \rangle, \tag{35}$$

where $j(t)$ is the particle current operator depending on time. For the Hamiltonian given in Eq. (1), the current operator reads

$$j(t) = \sum_{\mathbf{k},\alpha} \mathrm{v}^{\alpha}_{\mathbf{k}} c^{\dagger}_{\mathbf{k}\alpha} c_{\mathbf{k}\alpha}(t), \tag{36}$$

with $\mathrm{v}^{\alpha}_{\mathbf{k}} = \nabla \varepsilon^{\alpha}_{\mathbf{k}}$, where $\varepsilon^{\alpha}_{\mathbf{k}}$ are defined in Eq. (2). From the identity in Eq. (26) one can rewrite Eq. (35) as

$$\sigma(\omega) = \mathrm{Re}\frac{1}{\omega}\int_0^{\infty} dt e^{i\omega t} \langle [\tilde{j}(t), \tilde{j}(0)] \rangle_{\tilde{\mathcal{H}}}, \tag{37}$$

where

$$\tilde{j}(t) = \sum_{\mathbf{k},\alpha} \mathrm{v}^{\alpha}_{\mathbf{k}} \tilde{c}^{\dagger}_{\mathbf{k}\alpha} \tilde{c}_{\mathbf{k}\alpha}(t), \tag{38}$$

is the renormalized time-dependent current operator that is expressed in terms of the renormalized single quasi-particle operator depending on time $\tilde{c}_{\mathbf{k}\alpha}(t)$ estimated in Eq. (31). The average in Eq. (37) is formed with the completely renormalized Hamiltonian $\tilde{\mathcal{H}}$ in Eq. (20) or in the diagonal form in Eq. (21). Similar to the evaluation of the expectation values in Eqs. (32), one arrives at

$$\sigma(\omega) = \frac{1}{\omega}\sum_{\mathbf{k}\beta\beta'} A^{1}_{\mathbf{k}\beta\beta'} \delta\big(\omega + E^{\beta}_{\mathbf{k}} - E^{\beta'}_{\mathbf{k}}\big) + \frac{1}{\omega}\sum_{\substack{\mathbf{kpq} \\ \beta_{1,2}\beta'_{1,2}}} A^{2}_{\mathbf{kpq},\beta_{1,2}\beta'_{1,2}} \delta\big(\omega + E^{\beta_1}_{\mathbf{k}+\mathbf{p}} - E^{\beta'_1}_{\mathbf{k}} + E^{\beta_2}_{\mathbf{p}-\mathbf{q}} - E^{\beta'_2}_{\mathbf{p}}\big), \tag{39}$$

where

$$\begin{aligned}
A^{1}_{\mathbf{k}\beta\beta'} =& \sum_{\alpha\alpha'} \mathrm{v}^{\alpha}_{\mathbf{k}} \mathrm{v}^{\alpha'}_{\mathbf{k}} |\tilde{x}^{\alpha}_{\mathbf{k}}|^2 |\tilde{x}^{\alpha'}_{\mathbf{k}}|^2 u^{\alpha\beta}_{\mathbf{k}} u^{\alpha\beta'}_{\mathbf{k}} u^{\alpha'\beta'}_{\mathbf{k}} u^{\alpha'\beta}_{\mathbf{k}} \big[f\big(E^{\beta}_{\mathbf{k}}\big) - f\big(E^{\beta'}_{\mathbf{k}}\big)\big] \\
&- \frac{1}{N}\sum_{\mathbf{q},\alpha\alpha'\beta_1} \mathrm{v}^{\alpha}_{\mathbf{k}} \mathrm{v}^{\alpha'}_{\mathbf{k}} |\tilde{x}^{\alpha}_{\mathbf{k}}|^3 \tilde{y}^{\alpha}_{\mathbf{k},\mathbf{k}+\mathbf{q},\mathbf{q}} u^{\alpha\beta}_{\mathbf{k}} u^{\alpha\beta'}_{\mathbf{k}} u^{\alpha'\beta_1}_{\mathbf{k}+\mathbf{q}} u^{\alpha'\beta}_{\mathbf{k}} u^{-\alpha'\beta'}_{\mathbf{k}} u^{-\alpha'\beta_1}_{\mathbf{k}+\mathbf{q}} f\big(E^{\beta_1}_{\mathbf{k}+\mathbf{q}}\big)\big[f\big(E^{\beta}_{\mathbf{k}}\big) - f\big(E^{\beta'}_{\mathbf{k}}\big)\big] \\
&+ \frac{1}{N^2}\sum_{\substack{\mathbf{pq} \\ \alpha\alpha'\beta_1\beta_2}} \mathrm{v}^{\alpha}_{\mathbf{k}} \mathrm{v}^{\alpha'}_{\mathbf{q}} |\tilde{x}^{\alpha}_{\mathbf{k}}|^2 u^{\alpha\beta}_{\mathbf{k}} u^{\alpha\beta'}_{\mathbf{k}} |\tilde{y}^{\alpha'}_{\mathbf{qp},\mathbf{k}-\mathbf{q}}|^2 u^{\alpha'\beta'}_{\mathbf{k}} u^{\alpha\beta}_{\mathbf{k}} |u^{-\alpha'\beta_1}_{\mathbf{p}-\mathbf{k}+\mathbf{q}} u^{-\alpha'\beta_2}_{\mathbf{p}}|^2 f\big(E^{\beta_1}_{\mathbf{p}-\mathbf{k}+\mathbf{q}}\big)\big[1 - f\big(E^{\beta_2}_{\mathbf{k}}\big)\big]\big[f\big(E^{\beta}_{\mathbf{k}}\big) - f\big(E^{\beta'}_{\mathbf{k}}\big)\big] \\
&+ \frac{1}{N^3}\sum_{\substack{\mathbf{k'pq} \\ \alpha\alpha'\beta_1\beta_2}} \mathrm{v}^{\alpha}_{\mathbf{k}} \mathrm{v}^{\alpha'}_{\mathbf{q}} |\tilde{x}^{\alpha}_{\mathbf{k}}|^2 u^{\alpha\beta}_{\mathbf{k}} u^{\alpha\beta'}_{\mathbf{k}} \big\{ |\tilde{y}^{\alpha'}_{\mathbf{k'pq}}|^2 |u^{\alpha'\beta_1}_{\mathbf{k'}+\mathbf{q}} u^{-\alpha'\beta_2}_{\mathbf{p}}|^2 u^{-\alpha'\beta'}_{\mathbf{p}-\mathbf{q}} u^{\alpha'\beta}_{\mathbf{p}-\mathbf{q}} f\big(E^{\beta_1}_{\mathbf{k'}+\mathbf{q}}\big) f\big(E^{\beta}_{\mathbf{k}}\big)\big[1 - f\big(E^{\beta_2}_{\mathbf{p}}\big)\big] \\
&- |\tilde{y}^{\alpha'}_{\mathbf{k'kq}}|^2 |u^{\alpha'\beta_1}_{\mathbf{k'}+\mathbf{q}} u^{-\alpha'\beta_2}_{\mathbf{k}-\mathbf{q}}|^2 u^{-\alpha'\beta'}_{\mathbf{k}} u^{-\alpha'\beta'}_{\mathbf{k}} f\big(E^{\beta_1}_{\mathbf{k'}+\mathbf{q}}\big) f\big(E^{\beta_2}_{\mathbf{k}-\mathbf{q}}\big)\big[1 - f\big(E^{\beta'}_{\mathbf{k}}\big)\big] \big\},
\end{aligned} \tag{40}$$

$$\begin{aligned}
A^{2}_{\mathbf{kpq},\beta_{1,2}\beta'_{1,2}} =& \frac{1}{N^2}\sum_{\mathbf{pq},\alpha\alpha'} \mathrm{v}^{\alpha}_{\mathbf{k}} \tilde{x}^{\alpha}_{\mathbf{k}} \tilde{y}^{\alpha}_{\mathbf{kpq}} u^{\alpha\beta_1}_{\mathbf{k}+\mathbf{p}} u^{\alpha\beta'_1}_{\mathbf{k}} u^{-\alpha\beta_2}_{\mathbf{p}-\mathbf{q}} u^{\alpha'\beta'_2}_{\mathbf{p}} \big(\tilde{x}^{\alpha'}_{\mathbf{p}-\mathbf{q}} \tilde{y}^{\alpha'}_{\mathbf{p}-\mathbf{q},\mathbf{qp}} u^{\alpha'\beta'_2}_{\mathbf{p}} u^{\alpha'\beta_2}_{\mathbf{p}-\mathbf{q}} u^{-\alpha'\beta'_1}_{\mathbf{k}} u^{-\alpha'\beta_1}_{\mathbf{q}} - \tilde{x}^{\alpha'}_{\mathbf{k}+\mathbf{p}} \tilde{y}^{\alpha'}_{\mathbf{k}+\mathbf{p},-\mathbf{p},-\mathbf{q}} u^{\alpha'\beta'_1}_{\mathbf{k}+\mathbf{p}-\mathbf{q}} u^{\alpha'\beta_1}_{\mathbf{k}+\mathbf{p}} u^{-\alpha'\beta'_1}_{\mathbf{q}-\mathbf{p}} u^{-\alpha'\beta_1}_{-\mathbf{p}}\big) \\
&\times \big\{ f\big(E^{\beta_1}_{\mathbf{k}+\mathbf{p}}\big)\big[1 - f\big(E^{\beta'_1}_{\mathbf{k}}\big)\big]\big[f\big(E^{\beta_2}_{\mathbf{p}-\mathbf{q}}\big) - f\big(E^{\beta'_2}_{\mathbf{p}}\big)\big] + f\big(E^{\beta'_2}_{\mathbf{p}}\big)\big[1 - f\big(E^{\beta_2}_{\mathbf{p}-\mathbf{q}}\big)\big]\big[f\big(E^{\beta_1}_{\mathbf{k}+\mathbf{p}}\big) - f\big(E^{\beta'_1}_{\mathbf{k}}\big)\big] \big\}.
\end{aligned} \tag{41}$$

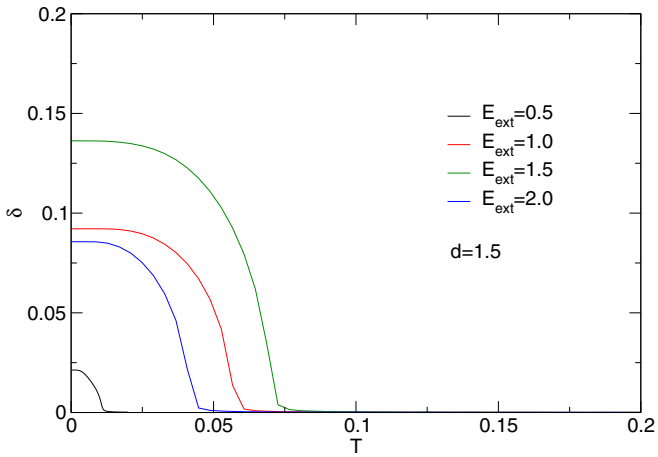

FIG. 1. Order parameter $\delta = (1/N)\sum_{\mathbf{k}} \delta_{\mathbf{k}}$ as a function of temperature T for dielectric thickness $d = 1.5$ with some values of external electric field E_{ext}.

The first line in Eq. (40) is the coherent contribution that describes excitations at the electronic quasiparticle energies $\tilde{E}^{\pm}_{\mathbf{k}}$. The remaining lines are incoherent contributions. Note that the coherent part reduces to the mean-field result when the renormalized quantities are replaced by the unrenormalized quantities.

IV. RESULTS AND DISCUSSION

To discuss the excitonic condensation state in the DLG structure within the PRM, the sets of renormalization Eqs. (15)–(17), (28), and (29) for the renormalized parameters would be solved self-consistently together with Eqs. (7) and (32) for the expectation values. Starting from some initial values of $n^{\alpha}_{\mathbf{k}}$ and $\delta_{\mathbf{k}}$, the renormalization equations are integrated in step by step $\Delta\lambda$ starting from $\lambda = \Lambda$. At $\lambda = 0$, the Hamiltonian and all single quasiparticle operators are completely renormalized. The expectation values then are recalculated by using Eqs. (32). The renormalization process is restarted until a convergence is achieved if all quantities are determined with a relative error less than 10^{-7}. In the numerical calculation, $\Delta\lambda$ was customarily chosen as $\Delta\lambda \approx 0.01$. Note here that instead of the hexagonal, the momentum space in our calculation is spanned in an equivalent triangular Brillouin zone specified by vectors given by $\mathbf{b}_1 = (2\pi/3a)(1, \sqrt{3})$ and $\mathbf{b}_2 = (2\pi/3a)(1, -\sqrt{3})$ [12]. Without loss of generality, in what follows, we choose $\gamma_0 = 1$ and $a = 1$ as units of energy and length, respectively. The interlayer Coulomb coupling constant $\kappa = 7$ is used to be applicable for the situation with SiO_2 substrate/dielectric ($\epsilon \simeq 4$) [19].

The excitonic condensation state is specified by a nonzero of the expectation value $\delta_{\mathbf{k}}$, indicating the hybridization between an electron on one layer and a hole in the other layer inducing the coherent state of the electron-hole pairs driven by the interlayer Coulomb attraction. Since the Coulomb interaction takes over for all momenta, we can evaluate $\delta = (1/N)\sum_{\mathbf{k}} \delta_{\mathbf{k}}$ standing for an order parameter considering a uniform excitonic condensate in DLG. Figure 1 shows the excitonic order quantity δ against the temperature T for some magnitude values of the external electric field E_{ext} at the dielectric thickness $d = 1.5$. By detuning the external electric field, the conduction band of the upper layer enters the valence band of the lower layer. That leads to a formation of excitons and the excitonic condensation can set in if the temperature is small enough. The scenario takes place first at the Dirac points and then shifts to the momenta around the special points by enhancing the electric field. Increasing the electric field would lead to a strong hybridization of the conduction and the valance electron bands. At a given sufficient large E_{ext}, one always finds a nonzero value of the excitonic order parameter indicating that the system stabilizes in the excitonic condensation state. Increasing temperature, the thermal fluctuations deplete the interlayer quantum coherence, and the order parameter decreases. Once the temperature is larger than a critical value, all bound pairs are damaged due to the thermal fluctuations, consequently, the system settles in the disorder, the so-called electron/hole plasma state. The critical value is called the excitonic transition temperature T_{C}. It is acceptable that the DLG is likely a 2D system and, of course, the critical temperature for exciton condensation would be zero. However, the system still survives in the superfluid state for temperatures smaller than the Kosterlitz-Thouless transition temperature T_{KT} [20,25]. Therefore, our finite-temperature results will be valid for $T \leqslant T_{\text{KT}}$ at least. Raising the external electric field, the excitonic condensate becomes more robust due to an enhancement of the overlap between the conduction band of the upper layer and the valance band of the lower layer. Note here that the Fermi level is always in the intersect of the conduction and valance bands. The number of electrons in the conduction band is increased, whereas the number of electrons in the valance band is decreased. Once the external electric field is large enough, numbers of the excitonic bound states get maxed and then exhaust if the electric field further increases with respect to decreasing the excitonic condensate critical temperature (comparing the green and blue lines in Fig. 1, for instance). The signature of the critical temperature depending on the external electric field for a given dielectric thickness will be discussed in detail in Fig. 5 below.

In Fig. 2, we discuss signatures of the excitonic condensation order parameter δ depending on temperature T at a given external electric field $E_{\text{ext}} = 1$ for some values of dielectric thickness d. At a given dielectric thickness d, one finds a similar behavior of the thermal fluctuations affecting on excitonic condensation state as addressed in Fig. 1. With increasing the dielectric thickness d between the upper layer and the lower layer, Fig. 2 shows us that the critical temperature is monotonously decreased; meanwhile, the excitonic condensation order parameter δ versus the dielectric thickness d at zero temperature (see the inset of the Fig. 2) is non-. Note here that, for a given value of the external electric field, increasing d, in one way, leads to increasing the chemical potential or enlarging the overlap between the conduction and valance bands but, in other ways, decreases the interlayer Coulomb interaction. The interactive influence of the dielectric thickness on the two factors directly affects the excitonic bound state. The nonmonotonous behavior of the δ at $T = 0$ thus might appear. When the dielectric thickness d is sufficiently large, $d \gtrsim 1$, the excitonic order parameter δ decreases more rapidly with increasing the temperature. That might be explained if one notes that once d is large, the Coulomb interaction

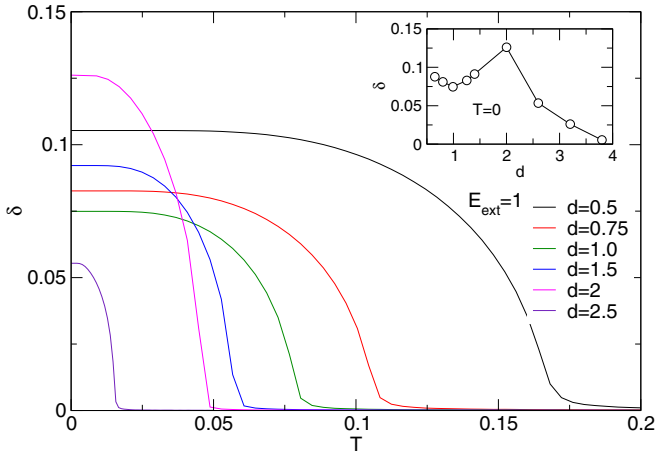

FIG. 2. Order parameter $\delta = (1/N)\sum_{\mathbf{k}} \delta_{\mathbf{k}}$ depending on the dielectric thickness d as a function of temperature T for an external electric field $E_{\text{ext}} = 1$. The inset shows a dependence of the order parameter δ on dielectric thickness d at zero temperature.

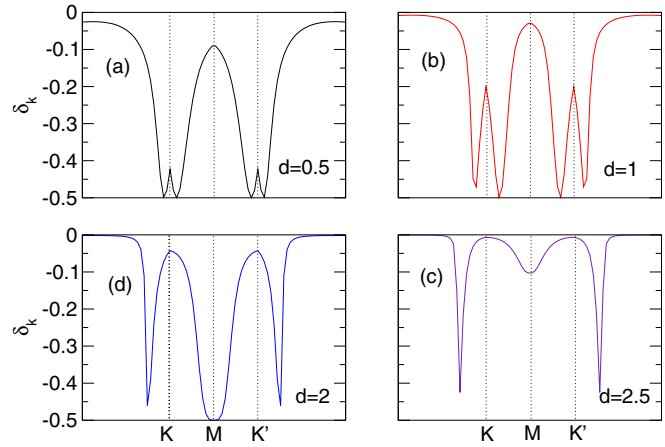

FIG. 4. Momentum distribution of the excitonic order parameter $\delta_{\mathbf{k}}$ for some dielectric thicknesses d at $T = 0$ and external electric field $E_{\text{ext}} = 1$ along the off-diagonal direction in the equivalent Brillouin zone. Dotted lines indicate some high symmetry points K, K', and M.

quickly diminishes [see Eq. (3)] and only a few pairs very close to the Fermi level around the momentum $\mathbf{q} \approx \mathbf{0}$ play an important role in forming the bound state. The bound state, therefore, is expeditiously depressed by the thermal fluctuations. The critical temperature for the excitonic condensation state, consequently, decreases with increasing the dielectric thickness d.

To understand the behavior of the excitonic condensation state at zero temperature versus the dielectric thickness d, in Fig. 3 we show the quasiparticle energies $E^{\alpha}_{\mathbf{k}}$ for some dielectric thicknesses d at $T = 0$ and external electric field $E_{\text{ext}} = 1$ along the off-diagonal direction in the equivalent Brillouin zone. At small d, the overlap of the conduction band on the upper layer with the valance band of the lower layer is small, however, the Coulomb interaction is large. The band gap thus is enlarged around a small deviation of the K points. In this

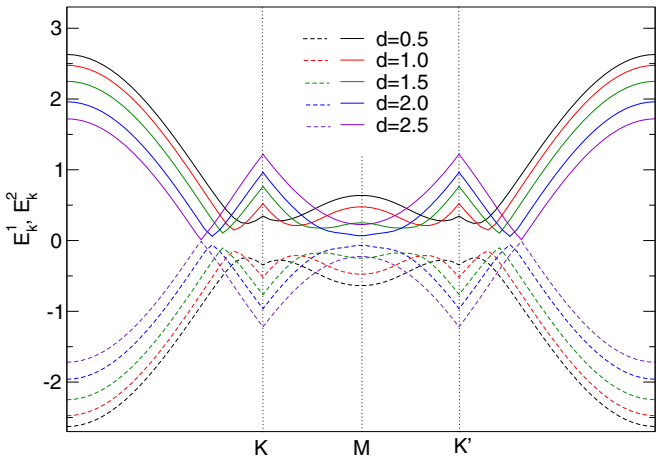

FIG. 3. Quasiparticle energies $E^1_{\mathbf{k}}$ (solid lines) and $E^2_{\mathbf{k}}$ (dashed lines) for some dielectric thicknesses d at $T = 0$ and external electric field $E_{\text{ext}} = 1$ along the off-diagonal direction in the equivalent Brillouin zone. Dotted lines indicate some high symmetry points K, K', and M.

case, one finds a maximum of the momentum distribution of the excitonic order parameter $\delta_{\mathbf{k}}$ [see Fig. 4(a)] close the Fermi level. The so-called Fermi momenta are very close to the K points. Enlarging d makes the conduction band shift down and the valance band move up. The Fermi momenta are thus shifted further far from the K points. Moreover, in this situation, the Coulomb interaction is reduced; consequently, the energy gap gets smaller. However, by enlarging d, some levels with momenta around the M point reach the Fermi level. The electrons and holes with that momenta might contribute to the formation of the excitons and stabilize the excitonic condensation state. For instance, at $d = 2$, one finds a large momentum distribution of the excitonic condensate order parameter $\delta_{\mathbf{k}}$ at the M point [see Fig. 4(c)]. That is a reason the excitonic order parameter δ gets maximum at $d = 2$, as shown in the inset of Fig. 2. Increasing d further, the Coulomb interaction gets smaller and only a small number of electrons and holes very close to the Fermi level play a role in the formation of the excitonic condensation state. The energy gap thus is small with a sharp excitonic condensate distribution around the Fermi momenta and the contribution of the quasiparticle around the M point is less important [see Fig. 4(d)]. In all cases, one always finds a sharp peak in the momentum distribution of the excitonic condensate order parameter $\delta_{\mathbf{k}}$ around the Fermi level. The excitonic condensation state in the system thus typifies the BCS type.

To summarize the interplay of the dielectric thickness d and external electric field E_{ext} affecting the stability of the excitonic condensation state under the influence of the thermal fluctuations, in Fig. 5 we show the phase diagram of the excitonic condensation state in the DLG system in the (T, E_{ext}) plane for some values of dielectric thicknesses d. At a given suitable set of the dielectric thickness d and external electric field E_{ext}, the excitonic condensate might be found at low temperatures. Once the temperature is larger than a critical value, the thermal fluctuations destroy the coherent bound state and the system is out of the order state. When the dielectric thickness is small, for instance, at $d = 0.5$,

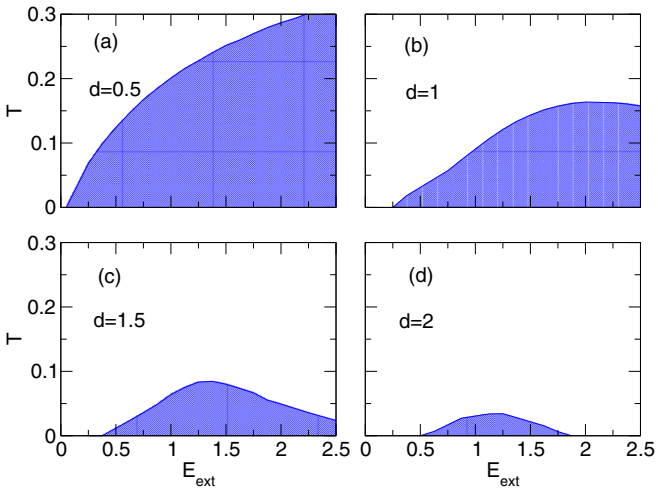

FIG. 5. Phase diagram of the excitonic condensate in DLG in the (T, E_{ext}) plane for different values of dielectric thickness d.

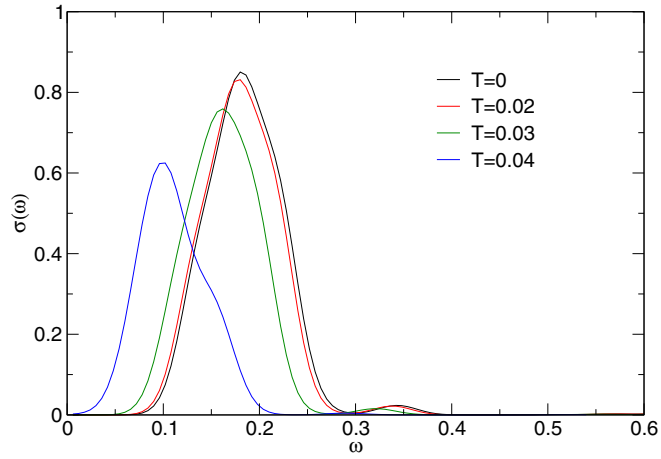

FIG. 6. Real part of the optical conductivity $\sigma(\omega)$ in the excionic condensation state at $E_{\text{ext}} = 1$, $d = 1.5$ for some different values of temperature T.

increasing the external electric field in a range of $E_{\text{ext}} \leqslant 2$, one finds the broaden window of the excitonic condensation state [see the Fig. 5(a)]. The condensate region sharply collapses when the two layers are separated further by a dielectric medium. Indeed, at the dielectric thickness $d = 1$, Fig. 5(b) illustrates a smaller dome of the excitonic condensation state by varying the external electric field. The excitonic condensation state only appears if the E_{ext} is sufficiently large. Increasing E_{ext} induces the development of the excitonic condensation regime with respect to enhancing the transition temperature of the condensation state. For $E_{\text{ext}} \approx 2$, the critical temperature gets maximum, the excitonic condensation regime then collapses once E_{ext} increases further. The position of E_{ext} at which the critical temperature gets maximum shifts to the left if the dielectric thickness d is larger [cf. Figs. 5(c) and 5(d)]. Even at $d = 2$, Fig. 5(d) shows us that the excitonic condensation state exists as a small island with $0.5 < E_{\text{ext}} < 2$. In this case, only a few electron-hole pairs very close to the Fermi level play a role in the formation of the bound coherent state.

Next, we discuss the optical properties of the excitonic condensate in DLG. Inspecting the signatures of the optical conductivity might give us valuable information about the quasiparticle properties, particularly regarding the quasiparticle dynamics. In Fig. 6, we present the real part of the optical conductivity $\sigma(\omega)$ at a given set of the dielectric thickness $d = 1.5$ and external electric field $E_{\text{ext}} = 1$ for some temperatures below the critical value (see the red line in Fig. 1). When the system settles in the excitonic condensation state, one always finds that the real part of the optical conductivity is nearly zero for the frequency ω smaller than a double of the excitonic condensate order parameter at the Fermi level δ_{kF}. In this range of the electron-hole continuum, the spectral weight of the optical conductivity is apparently diminished. However, at the edge of the electron-hole continuum or at the frequency $\omega \approx 2\delta_{kF}$, the optical response gets a maximum, then it quickly drops toward the normal state conductivity by increasing the frequency further. The sharp peak of the optical conductivity at the frequency $\omega = 2\delta_{kF}$ indicates the resonance state in the case of the strong hybridization between the electrons in the upper layer and the holes in the lower layer, with respect to the formation of the excitonic condensate. The presence of the hybridization or interorbital interaction delivers the peak in the optical conductivity spectrum and also the band gap in the quasiparticle energies. At the given set of E_{ext} and d the peak position of the optical spectrum shifts to the left with increasing temperature. This signature of the spectrum makes sense as we have mentioned that the excitonic condensation order parameter decreases by raising the thermal fluctuations.

To discuss influence of the interlayer dielectric thickness on the optical signatures in DLG, in Fig. 7 we show the real part of the optical conductivity $\sigma(\omega)$ at zero temperature $T = 0$ and external field $E_{\text{ext}} = 1$ for some dielectric thicknesses d. When d is small, at $d = 0.5$, for instance, the energy gap is largely opened, corresponding to the appearance of large frequency peaks in the optical conductivity spectrum. Increasing d, for instance, up to $d = 1$, the peaks shift to the

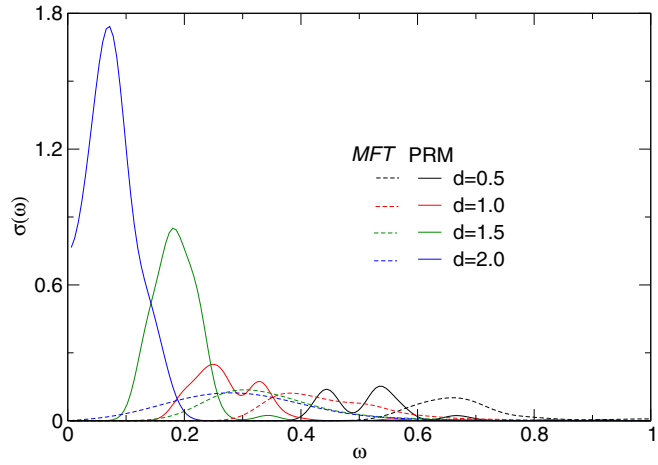

FIG. 7. Real part of the optical conductivity $\sigma(\omega)$ at zero temperature $T = 0$ and external field $E_{\text{ext}} = 1$ for some dielectric thicknesses d by use of PRM (solid lines) and MFT (dashed lines) for comparison.

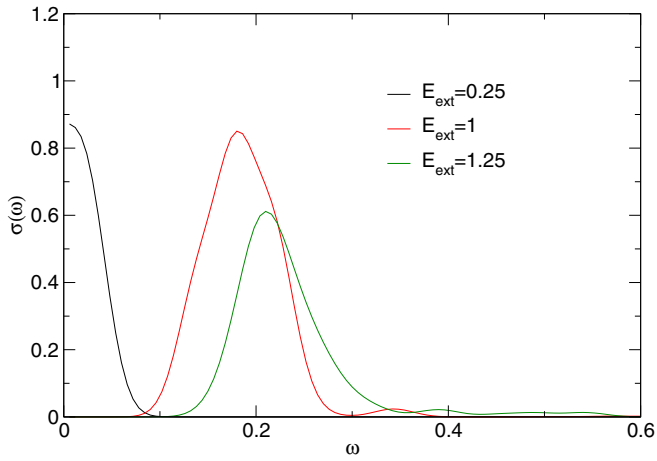

FIG. 8. Real part of the optical conductivity $\sigma(\omega)$ at zero temperature $T = 0$ and dielectric thickness $d = 1.5$ for some external electric fields E_{ext}.

left due to the shrink of the energy gap close to the Fermi level. In this range of the dielectric thickness, one finds a two-peak signature of the optical conductivity. The two-peak structure might be induced from the contribution of the incoherent parts based on the PRM. Note here that in the approach of the mean-field theory (MFT), i.e., all the fluctuation contributions are eliminated; the two-peak structure does not appear (see the dashed lines in Fig. 7). With increasing d, the Coulomb interaction is reduced, the peak with higher frequency is less significant, and finally disappears when d is large enough (for instance, at $d \geqslant 2$). From Fig. 7, one also learns that, due to the contribution of the renormalization, the optical conductivity spectrums shift to the left with lower frequencies. That signature indicates that the excitonic condensate order parameter evaluated by the present PRM with all fluctuation contributions deviates from the overestimated value evaluated by the original mean-field approximation.

To gain further insight about the external electric field influence in the optical properties of the excitonic condensation state in DLG, we show in Fig. 8 the real part of the optical conductivity at zero temperature and dielectric thickness $d = 1.5$ for some values of E_{ext}. For a given dielectric thickness d, the Coulomb interaction is fixed, thus if the external electric field is small the system might not be stabilized in the excitonic condensation state and no peak signature at a finite frequency can be found in the optical conductivity spectrum. The situation is changed once the external electric field is large enough and the system settles in the excitonic condensation state. In this case, the optical conductivity displays the peak at a finite frequency corresponding to the double of the energy gap at the Fermi level.

V. CONCLUDING REMARKS

To conclude, we have analyzed the excitonic condensation state in a DLG system by means of a PRM adapting to a generic graphene bilayer model, so the fluctuations due to the interlayer Coulomb interaction between an electron in the upper layer and a hole in the lower layer are taken into account. In the calculation, we have supposed that electron-hole pair formation and condensation might appear in the DLG system at least at zero temperature if a finite external electric field is applied. In doing so, we have derived a set of self-consistent equations permitting us to solve numerically the excitonic condensate order parameters once the renormalization contributions are involved. In the feature of the projector-based renormalization approach, we also released an analytical formula for the real part of the optical conductivity. The signature of the optical properties of the system in the condensation state was then addressed. For a given dielectric medium embedded in between two layers, one finds a dome of the excitonic condensation state in the influence of the external electric field and the thermal fluctuations. The dome is rapidly suppressed when the dielectric thickness is enlarged. As a function of the dielectric thickness, we also found a nonmonotonous behavior of the excitonic condensate order parameter at zero temperature. In the present paper, we also presented signatures of the optical conductivity to address the dynamical properties of the excitonic condensation state in DLG by which the real part of the optical conductivity is considered, that rises at a sharp peak at a frequency equal to twice the excitonic condensate order parameter. Once the dielectric thickness is small with respect to large Coulomb interaction, the renormalization induces the two-peak signatures of the optical conductivity spectrum in the condensation state. Enlarging the dielectric thickness, the spectrum recovers the one-peak signature as found by the original MFT. Our findings thus have addressed in detail the phase structure of the excitonic condensation state in the DLG and especially released the dynamical properties of the condensate state in the singatures of the optical conductivity. In the framework of the projector-based renormalization approach, all contributions of the quantum fluctuations to the phase transition are taken into account. The results are promising for the profound understanding of the excitonic condensation state in double-layer systems and also in the semimetal-semiconductor transition materials, in general.

ACKNOWLEDGMENTS

This research is funded by the Vietnam National Foundation for Science and Technology Development (NAFOSTED) under Grant No. 103.01-2019.306.

[1] D. Jérome, T. M. Rice, and W. Kohn, Phys. Rev. **158**, 462 (1967).

[2] P. B. Littlewood, P. R. Eastham, J. M. J. Keeling, F. M. Marchetti, B. D. Simons, and M. H. Szymanska, J. Phys.: Condens. Matter **16**, S3597 (2004).

[3] N. F. Mott, Philos. Mag. **6**, 287 (1961).

[4] R. Knox, in *Solid State Physics*, edited by F. Seitz and D. Turnbull (Academic Press, New York, 1963), p. Suppl. 5, p. 100.

[5] H. Cercellier, C. Monney, F. Clerc, C. Battaglia, L. Despont, M. G. Garnier, H. Beck, P.Aebi, L. Patthey, H. Berger, and L. Forró, Phys. Rev. Lett. **99**, 146403 (2007).

[6] C. Monney, H. Cercellier, F. Clerc, C. Battaglia, E. F. Schwier, C. Didiot, M. G. Garnier, H. Beck, P. Aebi, H. Berger, L. Forró, and L. Patthey, Phys. Rev. B **79**, 045116 (2009).

[7] J. P. Eisenstein and A. H. MacDonald, Nature **432**, 691 (2004).

[8] J. A. Seamons, C. P. Morath, J. L. Reno, and M. P. Lilly, Phys. Rev. Lett. **102**, 026804 (2009).

[9] X. Liu, K. Watanabe, T. Taniguchi, B. I. Halperin, and P. Kim, Nat. Phys. **13**, 746 (2017).

[10] J. I. A. Li, T. Taniguchi, K. Watanabe, J. Hone, and C. R. Dean, Nat. Phys. **13**, 751 (2017).

[11] J. I. A. Li, Q. Shi, Y. Zeng, K. Watanabe, T. Taniguchi, J. Hone, and C. R. Dean, Nat. Phys. **15**, 898 (2019).

[12] A. H. Castro Neto, F. Guinea, N. M. R. Peres, K. S. Novoselov, and A. K. Geim, Rev. Mod. Phys. **81**, 109 (2009).

[13] N. M. R. Peres, Rev. Mod. Phys. **82**, 2673 (2010).

[14] D. S. L. Abergel, V. Apalkov, J. Berashevich, K. Ziegler, and T. Chakraborty, Adv. Phys. **59**, 261 (2010).

[15] K. S. Novoselov, A. K. Geim, S. V. Morozov, D. Jiang, M. I. Katsnelson, I. V. Grigorieva, S. V. Dubonos, and A. A. Firsov, Nature **438**, 197 (2005).

[16] Y. Zhang, Y.-W. Tan, H. L. Stormer, and P. Kim, Nature **438**, 201 (2005).

[17] K. S. Novoselov, E. McCann, S. V. Morozov, V. I. Fal'ko, M. I. Katsnelson, U. Zeitler, D. Jiang, F. Schedin, and A. K. Geim, Nat. Phys. **2**, 177 (2006).

[18] T. Ohta, A. Bostwick, T. Seyller, K. Horn, and E. Rotenberg, Science **313**, 951 (2006).

[19] Y. E. Lozovik and A. A. Sokolik, JETP Lett. **87**, 55 (2008).

[20] C.-H. Zhang and Y. N. Joglekar, Phys. Rev. B **77**, 233405 (2008).

[21] L. A. Ponomarenko, A. K. Geim, A. A. Zhukov, R. Jalil, S. V. Morozov, K. S. Novoselov, I. V. Grigorieva, E. H. Hill, V. V. Cheianov, V. I. Fal'ko, K. Watanabe, T. Taniguchi, and R. V. Gorbachev, Nat. Phys. **7**, 958 (2011).

[22] T. Stauber and G. Gómez-Santos, Phys. Rev. B **85**, 075410 (2012).

[23] K. S. Novoselov, A. K. Geim, S. V. Morozov, D. Jiang, Y. Zhang, S. V. Dubonos, I. V. Grigorieva, and A. A. Firsov, Science **306**, 666 (2004).

[24] R. Dillenschneider and J. H. Han, Phys. Rev. B **78**, 045401 (2008).

[25] H. Min, R. Bistritzer, J. J. Su, and A. H. MacDonald, Phys. Rev. B **78**, 121401(R) (2008).

[26] R. Nandkishore and L. Levitov, Phys. Rev. Lett. **104**, 156803 (2010).

[27] N. Hao, P. Zhang, and Y. Wang, Phys. Rev. B **84**, 155447 (2011).

[28] V. N. Phan and H. Fehske, New J. Phys. **14**, 075007 (2012).

[29] L. V. Keldysh and A. N. Kozlov, Sov. Phys. JETP **27**, 521 (1968).

[30] S. Sykora, A. Hübsch, and K. W. Becker, Phys. Rev. B **102**, 165122 (2020).

[31] K. G. Wilson, Phys. Rev. **140**, B445 (1965).

[32] K. G. Wilson, Rev. Mod. Phys. **47**, 773 (1975).

[33] K. G. Wilson, Rev. Mod. Phys. **55**, 583 (1983).

[34] F. Wegner, Ann. Phys. (Leipzig) **506**, 77 (1994).

[35] S. D. Glazek and K. G. Wilson, Phys. Rev. D **48**, 5863 (1993).

[36] S. D. Glazek and K. G. Wilson, Phys. Rev. D **49**, 4214 (1994).

[37] V. N. Phan, K. W. Becker, and H. Fehske, Phys. Rev. B **81**, 205117 (2010).

[38] V. N. Phan, H. Fehske, and K. W. Becker, Europhys. Lett. **95**, 17006 (2011).

[39] V.-N. Phan, K. W. Becker, and H. Fehske, Phys. Rev. B **93**, 075138 (2016).

[40] K. W. Becker, H. Fehske, and V.-N. Phan, Phys. Rev. B **99**, 035304 (2019).

[41] S. Sykora and K. W. Becker, Phys. Rev. B **80**, 014511 (2009).

[42] V.-N. Phan, Phys. Rev. B **101**, 245120 (2020).

[43] K. Sugimoto, S. Nishimoto, T. Kaneko, and Y. Ohta, Phys. Rev. Lett. **120**, 247602 (2018).

[44] D. Ihle, M. Pfafferott, E. Burovski, F. X. Bronold, and H. Fehske, Phys. Rev. B **78**, 193103 (2008).

[45] H. Li, J. Otsuki, M. Naka, and S. Ishihara, Phys. Rev. B **101**, 125117 (2020).

[46] Y. Murakami, D. Golež, T. Kaneko, A. Koga, A. J. Millis, and P. Werner, Phys. Rev. B **101**, 195118 (2020).

[47] L. Yang, Nano Lett. **11**, 3844 (2011).

[48] L. Yang, J. Deslippe, C.-H. Park, M. L. Cohen, and S. G. Louie, Phys. Rev. Lett. **103**, 186802 (2009).

[49] K. V. Germash and D. V. Fil, Phys. Rev. B **93**, 205436 (2016).

[50] K. V. Germash and D. V. Fil, Europhys. Lett. **118**, 67008 (2017).

[51] K. V. Germash and D. V. Fil, Phys. Rev. B **99**, 125412 (2019).

[52] G. D. Mahan, *Many-Particle Physics* (Kluwer Academic/ Plenum Publishers, New York, 2000).

[53] K. W. Becker, A. Hübsch, and T. Sommer, Phys. Rev. B **66**, 235115 (2002).